

Investigating TNS4 in the Colorectal Tumor Microenvironment Using 3D Spheroid Models of Invasion

Teresa P. Raposo,* Susanti Susanti, and Mohammad Ilyas

TNS4 (Tensin 4 or Cten) is a putative oncogene in colorectal cancer (CRC) with a role in regulating cell adhesion, motility, invasion, and epithelial to mesenchymal transition (EMT). The objective is to study the role of TNS4 in CRC using more realistic models of the tumor microenvironment. CRC cells expressing TdTomato protein and shTNS4/shLUC hairpin oligos are grown in 3D spheroids with and without cancer-associated fibroblasts (CAFs). Adhesiveness to collagen I and CAFs is assessed in 2D and cell proliferation, volume, and invasion are assessed in 3D conditions. The role of TNS4 knockdown in gefitinib chemosensitivity and epidermal growth factor receptor (EGFR) and Ras protein levels are also tested. In general, TNS4 knockdown increases cell proliferation in cell lines producing compact spheroids. The addition of CAFs in spheroids supports CRC cell proliferation, whereas CAFs themselves do not proliferate, but increases ECM degradation. TNS4 knockdown reduces adhesiveness and 3D invasion and disrupts EGFR signaling which results in increased sensitivity to Gefitinib. In conclusion, in a 3D spheroid model, TNS4 inhibits cell proliferation and promotes cell invasion into the ECM, possibly by adhesion to the ECM and stromal cells. TNS4 knockdown enhances sensitivity to the EGFR inhibitor gefitinib and may be helpful for Kirsten ras oncogene homolog mutant CRC patients.


1. Introduction

TNS4 (tensin4) or Cten (C-terminal tensin-like) is a tensin localized to focal adhesion sites where it has a role in the dynamics

Dr. T. P. Raposo, Dr. S. Susanti, Prof. M. Ilyas
Division of Cancer and Stem Cells
School of Medicine
University of Nottingham
Queen's Medical Centre
Nottingham, NG7 2UH, UK
E-mail: rapteresa@gmail.com

Dr. T. P. Raposo, Dr. S. Susanti, Prof. M. Ilyas
Nottingham Molecular Pathology Node
University of Nottingham
UK

Dr. S. Susanti
Department of Pharmacology and Clinical Pharmacy
Faculty of Pharmacy
University of Muhammadiyah Purwokerto
Banyumas, Central Java 53182, Indonesia

 The ORCID identification number(s) for the author(s) of this article can be found under <https://doi.org/10.1002/adbi.202000031>.

© 2020 The Authors. Published by WILEY-VCH Verlag GmbH & Co. KGaA, Weinheim. This is an open access article under the terms of the Creative Commons Attribution License, which permits use, distribution and reproduction in any medium, provided the original work is properly cited.

DOI: 10.1002/adbi.202000031

of cell movement and adhesion by linking integrins and scaffold proteins to the actin cytoskeleton and the extracellular matrix (ECM).^[1,2]

During the past decade, TNS4 has been suggested as a putative oncogene due to its overexpression in a vast range of cancer types: breast,^[3] colorectal,^[4,5] hepatocellular carcinoma,^[6] melanoma,^[7] oesophagogastric adenocarcinoma,^[8] gastric,^[9,10] pancreatic,^[5] thymoma,^[11] and lung cancer.^[12]

Even though TNS4 has been identified as an oncogene in a number of cancers, the mechanisms regulating its role in motility, invasion, and metastasis are still under investigation.

In colorectal cancer (CRC) cell lines, TNS4 has been shown to induce epithelial to mesenchymal transition (EMT) by repressing E-cadherin and to significantly increase migration and invasion.^[4] More recently, a role for TNS4 in selectively mediating TGF- β -induced EMT in CRC cell lines has been reported. In the

absence of TNS4, the effects of TGF- β stimulation on inducing motility and invasion were abrogated, but TGF- β -induced proliferation was not affected.^[13] Furthermore, TNS4-mediated Src stabilization was found to be the responsible for EMT induction in CRC cell lines.^[14] Nude mice receiving a splenic injection of TNS4 overexpressing HCT116 cells have produced larger splenic tumors and hepatic metastatic nodules compared to the control group.^[15] However, thus far, studies demonstrating the role of TNS4 in syngeneic or immunocompetent animal models of CRC invasion and metastasis in vivo are still lacking.

The use of 3D in vitro models may fill in this gap by providing an enriched tumor microenvironment with improved cell interactions and ECM which better mimics the in vivo context and which may provide a better measure of drug response.^[16–20] Amongst the 3D in vitro models available for CRC, recellularized CRC scaffolds have been suggested as a useful preclinical patient-derived tool that could predict in vitro the success of future therapies administered to the patient.^[21] However, due to its uniqueness and complexity, this method may not be as practical as heterotypic spheroids for drug screening. Addition of stromal cell types such as cancer-associated fibroblasts (CAFs) to 3D models substantially supports growth of cancer cell lines and may also promote invasion and metastasis by guiding cancer cells at the invasive edge.^[22] Interactions between tumor and stroma are difficult to study in vivo due to limitations in tissue accessibility, in vivo monitoring and selection of specific intercellular interactions.^[23]

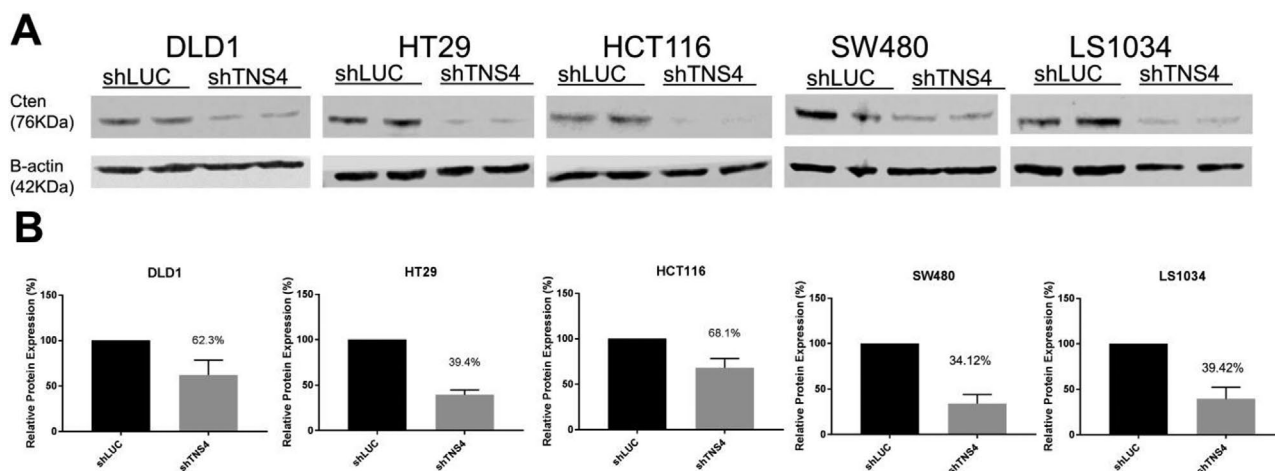


Figure 1. A) Western blot and B) respective densitometry showing a decrease in TNS4 expression achieved for shTNS4 stable knockdowns in DLD1 (62.3%), HT29 (39.4%), HCT116 (68.1%), SW480 (34.1%), and LS1034 (39.42%) cell lines relative to the loading control (β -Actin) and normalized to their shLUC (luciferase control, 100%). Two independent protein lysates were tested.

In this study we aim first to explore the role of TNS4 in heterotypic interactions between cancer cells and CAFs within the in vitro 3D spheroid tumor microenvironment, and second to validate the role of TNS4 in CRC proliferation and invasion in the same model. To this end, we have used stable lentiviral TNS4 and Luciferase control knockdowns of CRC cell lines expressing TdTomato fluorescent protein, alone or with cancer-associated fibroblasts in mixed spheroids. Expression of fluorescent TdTomato was used to measure the growth of CRC cells within the spheroid and GFP-tagged CAFs allowed imaging of CAFs invasion in the spheroids.

2. Results

2.1. Stable TNS4 Knockdown CRC Cell Lines

A stable knockdown of TNS4 was achieved by lentiviral transduction of colorectal cell lines, which is demonstrated by western blot on **Figure 1**. Following TNS4 stable knockdown, transduction with TdTomato lentivirus allowed us to follow the growth of the CRC cell population within the spheroids by using a conventional fluorescent plate reader to detect expression of TdTomato fluorescent protein.

The spheroid formation method used revealed different morphologies between CRC cell lines. Whilst DLD1, HT29 and HCT116 formed compact spheroids of round uniform shape, SW480, and SW620 produced aggregates and LS1034 produced a globous irregular shape. (Figure S1, Supporting Information).

2.2. TNS4 Knockdown Reduces Adhesiveness

In the attempt to explain the observed differences in spheroid size and growth we have assessed the ability of shTNS4 and shLUC CRC cells to adhere to ECM collagen type I, which would normally be secreted by CAFs, or CAFs themselves, by performing adapted adhesion assays in collagen type I coated plates or using CAFs as an adhesion substrate.

Whereas a tendency for reduced adhesion to collagen type I could be observed for all shTNS4 CRC cell lines, the difference to shLUC controls was only significant in HT29 ($p = 0.0205$) and SW480 ($p = 0.0245$) (**Figure 2A**). By repeating the adhesion assay over a layer of CAFs, statistically significant reduced attachment of shTNS4 versus shLUC was noted for DLD1 ($p = 0.0062$), HCT116 ($p = 0.0068$), HT29 ($p = 0.0145$), and LS1034 ($p = 0.0284$) (**Figure 2B**).

The reduced adhesion to CAFs upon TNS4 knockdown could have an effect in the expansion and paracrine growth signaling depending on cell-to-cell contact between CAFs and CRC cells, leading to increased fluorescence signal in shTNS4 versus shLUC + CAFs spheroids. Conversely, a reduced spheroid volume seen in shTNS4 + CAFs compared to shLUC + CAFs could be caused by increased compactness of the CRC cells, unsupported by a CAFs scaffold.

2.3. TNS4 Knockdown in 3D Spheroids Affects Proliferative Rates

To assess the growth of the CRC cell population within the spheroid, TdTomato fluorescence was measured daily over 7 days.

The SW620^{ΔCten} variant, in which TNS4 was deleted by using a CRISPR-Cas9 system, consistently showed increased spheroid growth when compared to its parental SW620 cell line ($p < 0.0001$) (**Figure 3A**, **Table 1A**). For both SW480 and LS1034 cell lines, the shTNS4 variant spheroids showed significantly reduced growth when compared to shLUC control spheroids (**Figure 3B,C**). In DLD1, HCT116 and HT29, shTNS4 variants produced spheroids with slightly increased proliferation, but which was only significant for HCT116 and HT29 ($p < 0.0001$) (**Figure 3D,E,F** and **Table 1D,E,F**).

Regarding the influence of CAFs in spheroid growth, a statistically significant increase in the growth of CRC cells in the spheroids was observed in SW620, SW480, and DLD1 when comparing shTNS4 variants with or without added CAFs at a 1:1 proportion (**Table 1A,B,D**). Interestingly, in LS1034 and HT29 (**Table 1C,F**), the promoting effect of CAFs was not seen in

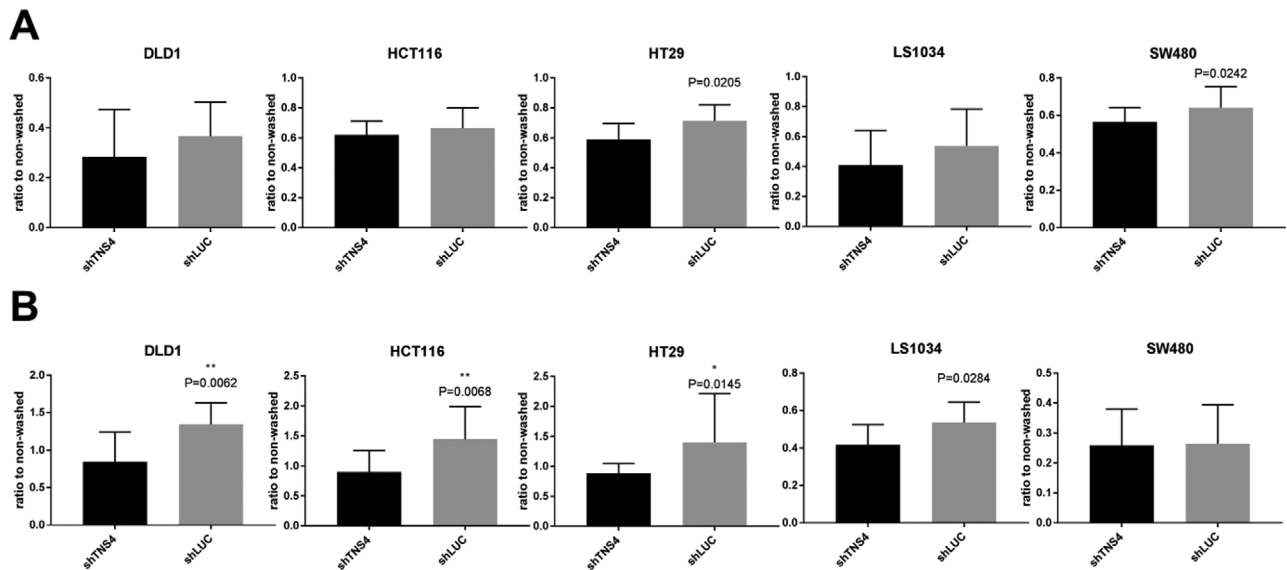


Figure 2. Adhesion assay of shTNS4 and shLUC CRC cells to A) collagen type I and B) CAFs feeder layer. Mann–Whitney statistical test was performed to evaluate differences between shTNS4 and shLUC CRC cells. $N = 12$ replicates and results shown are representative of two independent experiments. Statistically significant p -values are presented on top of the respective shTNS4 bars, in cases where statistically significant differences were not present, irrelevant p -values are omitted.

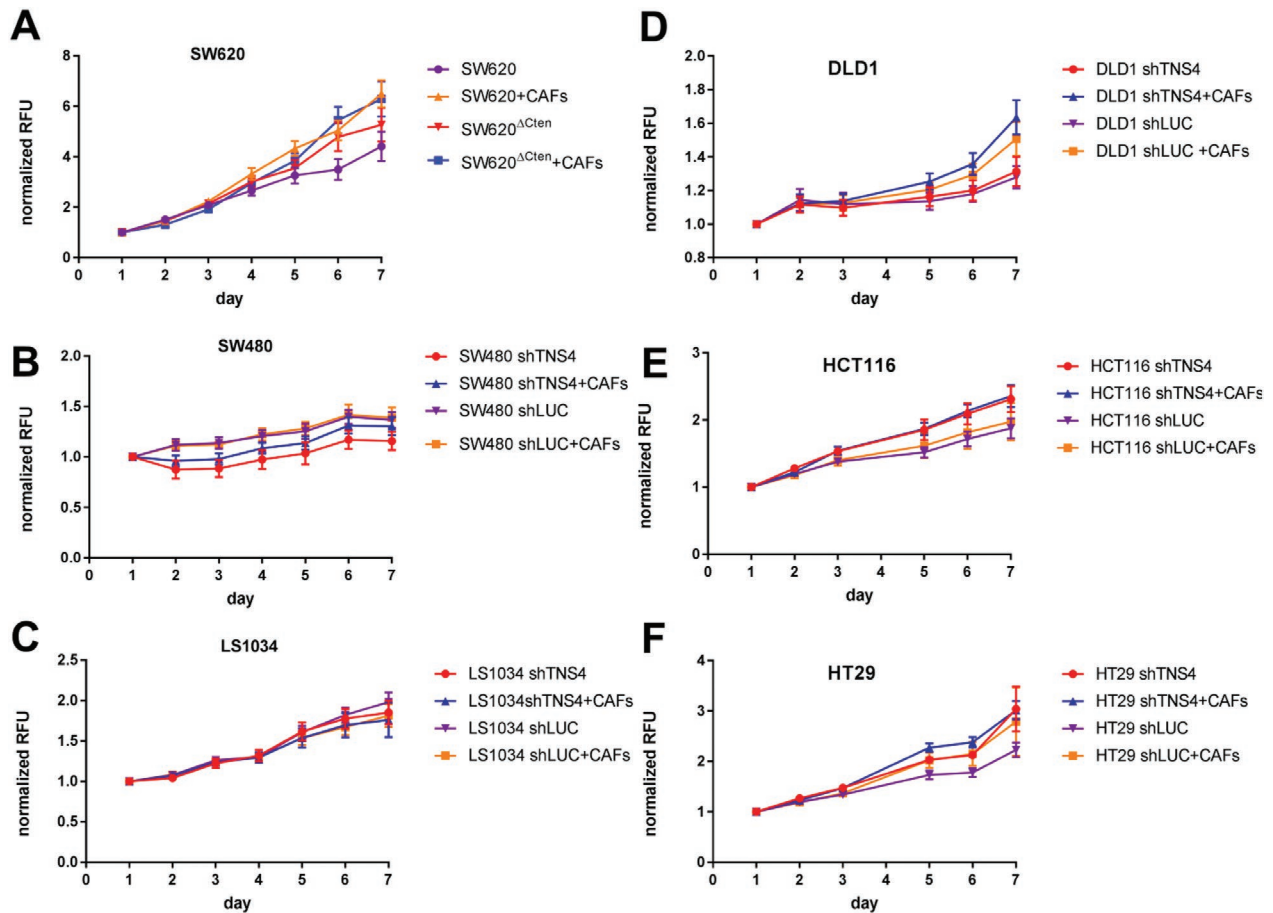


Figure 3. Mean \pm St dev of relative TdTomato fluorescence read-outs (540em–590ex nm) for spheroids composed of colorectal cell lines stably knock-down for TNS4 (shTNS4), luciferase control (shLUC) with and without addition of cancer-associated fibroblasts (CAFs). Graphs are representative of 12 replicates per condition and two independent experiments were carried out (the respective statistical analysis for this figure is shown on Table 1).

Table 1. Statistical analysis of TdTomato mean fluorescence readings at day 7 for spheroids composed of CRC cell lines with and without CAFs. For each condition $N = 12$ replicates and results are representative of two experiments. Two-way ANOVA statistical test with multiple comparisons by Tukey's test was performed, a p -value < 0.05 was considered statistically significant.

Tdtomato relative fluorescence multiple comparisons at day 7		
	Mean diff.	Adjusted p value
A)		
SW620 vs. SW620 + CAFs (1:1)	-2.085	<0.0001
SW620 vs. SW620 ^{DCTen}	-0.8601	<0.0001
SW620 ^{DCTen} vs. SW620 ^{DCTen} + CAFs	-1.022	<0.0001
SW620+CAF vs. SW620 ^{DCTen} + CAFs	0.2036	0.4229
B)		
SW480 shTNS4 vs. SW480 shTNS4 + CAFs	-0.1476	<0.0001
SW480 shTNS4 vs. SW480 shLUC	-0.209	<0.0001
SW480 shTNS4 + CAFs vs. SW480 shLUC + CAFs	-0.08405	0.0197
SW480 shLUC vs. SW480 shLUC + CAFs	-0.02262	0.8611
C)		
LS1034 shTNS4 vs. LS1034shTNS4 + CAFs	0.09316	0.0526
LS1034 shTNS4 vs. LS1034 shLUC	-0.1275	0.0029
LS1034shTNS4 + CAFs vs. LS1034 shLUC + CAFs	-0.05505	0.4299
LS1034 shLUC vs. LS1034 shLUC + CAFs	0.1657	<0.0001
D)		
DLD1 shTNS4 vs. DLD1 shTNS4 + CAFs	-0.322	<0.0001
DLD1 shTNS4 vs. DLD1 shLUC	0.03376	0.4726
DLD1 shTNS4 + CAFs vs. DLD1 shLUC + CAFs	0.1275	<0.0001
DLD1 shLUC vs. DLD1 shLUC +CAFs	-0.2283	<0.0001
E)		
HCT116 shTNS4 vs. HCT116 shTNS4 + CAFs	-0.04509	0.8057
HCT116 shTNS4 vs. HCT116 shLUC	0.4322	<0.0001
HCT116 shTNS4 + CAFs vs. HCT116 shLUC + CAFs	0.3812	<0.0001
HCT116 shLUC vs. HCT116 shLUC + CAFs	-0.0961	0.2243
F)		
HT29 shTNS4 vs. HT29 shTNS4 + CAFs	0.0251	0.9859
HT29 shTNS4 vs. HT29 shLUC	0.8126	<0.0001
HT29 shTNS4 + CAFs vs. HT29 shLUC + CAFs	0.2259	0.0176
HT29 shLUC vs. HT29 shLUC + CAFs	-0.5616	<0.0001

shTNS4 spheroids, but only in the presence of normal TNS4 expression in the shLUC spheroids (Figure 3C,F).

When comparing shTNS4 and shLUC co-cultured with CAFs, a significant growth boosting effect can be perceived for DLD1, HCT116, and HT29 (Figure 3D–F, Table 1D–F), in which spheroids composed of shTNS4 CRC cells with CAFs grow more than their control spheroids shLUC with CAFs. In CRC cell lines producing loose spheroid aggregates (SW620, SW480, and LS1034) this effect is not observed (Figure 3 and Table 1).

Regarding differences observed in terms of whole spheroid volume, these could only be measured in those cell lines forming round compact spheroids (DLD1, HCT116, and HT29), in which

the estimation made by approximation to the volume of a sphere is valid (Figure S1, Supporting Information, illustrates the spheroid morphology in the different cell lines used in this study). To normalize volumetric data, measurements taken on the second day were chosen for HCT116 and HT29, as spheroids of these cell lines only acquire a compact round shape later than DLD1. In HCT116 shTNS4 and shLUC variants as well as in DLD1 shLUC, addition of CAFs promoted spheroid growth in volume, only the difference between DLD1 shTNS4 and DLD1 shTNS4 + CAFs was not statistically significant (Figure 4A, Table 2A). However, in HT29, addition of CAFs seemed to reduce whole spheroid volume, possibly by contraction or increased compactness of the spheroid around CAFs (Figure 4C, Table 2C). When grown in low adherence conditions, CAFs form small spheroids and do not expand their volume, apparently in a quiescent state (Figure 3).

2.4. TNS4 Knockdown Reduced 3D Invasion and Response to CAFs-Driven Invasion

By performing 3D invasion assays measuring specific ECM degradation without quenching of DQ BSA green we were able to isolate matrix invasion from changes in spheroid size due to a variation in cell proliferation.

Comparing CRC spheroids, there was a significant decrease in 3D invasion in shTNS4 versus shLUC spheroids in both DLD1 ($p = 0.0434$) and HCT116 ($p = 0.0281$), but not in HT29 (Figure 5A). In general, addition of CAFs to form mixed population spheroids increased ECM degradation and invasion, although this was not always a statistically significant effect. An exception to CAFs' promotion of ECM degradation and invasion was observed with HT29 shTNS4 cells (Figure 5A and D), whereas a significant effect was observed for HT29 shLUC versus HT29 shLUC + CAFs ($p = 0.0070$). Interestingly, HT29 was the only CRC cell line where matrix degradation and invasion in shLUC + CAFs was superior to that of shTNS4 + CAFs cells ($p = 0.0055$), suggesting a particular effect of TNS4 expression in the interaction with CAFs.

2.5. TNS4 Knockdown Sensitizes CRC Cells to EGFR Inhibition Treatment

We and others have shown that TNS4 is an effector of the EFGR-KRAS-MAPK signaling pathway. This prompted us to investigate whether removing TNS4 could affect the activity of anti-EGFR drugs such as Gefitinib (which inhibits the kinase domain of EGFR). We investigated this in both 2D and 3D models.

Overall, we observed that knockdown of TNS4 resulted in increased chemosensitivity to gefitinib in all cell lines. This was seen in both assays, but the effect was more pronounced in 3D spheroids (Figure 6A,B). Gefitinib treatment alone in shTNS4 transduced cells reduced expression of EGFR, RAS, and TNS4, thereby confirming that TNS4 forms part of this signaling pathway (Figure 6C; Figure S2, Supporting Information). Interestingly, TNS4 knockdown resulted in higher EGFR levels than in shLUC controls suggesting a negative feedback loop between TNS4 and EGFR.

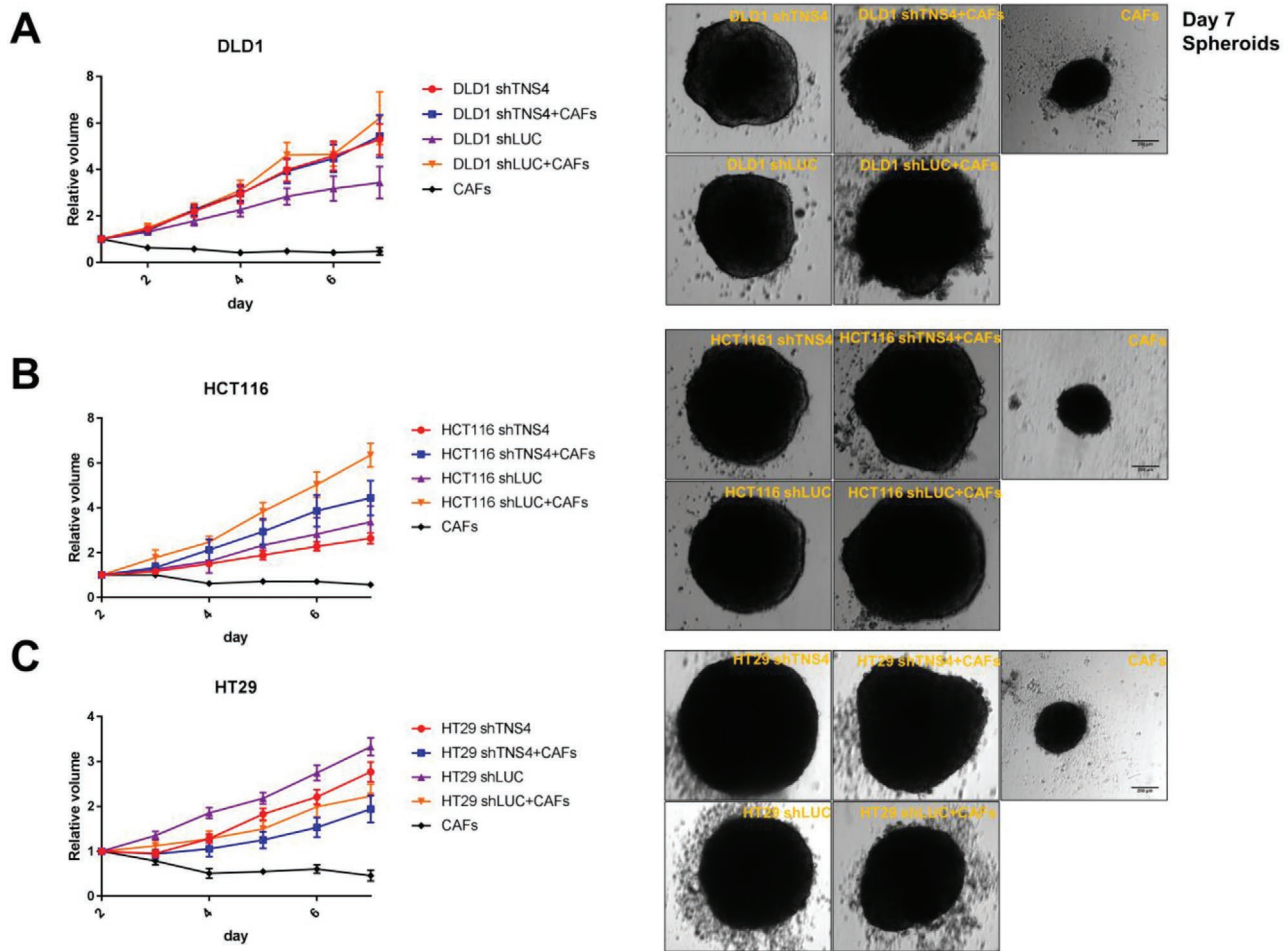


Figure 4. Volumetric measurements of spheroid growth in A) DLD1, B) HCT116, and C) HT29 CRC cell lines and representative images of spheroids composed of shTNS4/shLUC variants with or without added CAFs at day 7 (The respective statistical analysis for this figure is shown on Table 2).

3. Discussion

TNS4 overexpression has been reported in a number of cancers [3,7,8,24] although in CRC in vitro studies have not shown a role for TNS4 in cell proliferation. These were always performed in 2D settings, omitting the presence of an enriched tumor microenvironment with increased cell-to-cell interactions and supporting stromal cells. Only recently it has been reported that in HeLa cells, TNS4 transient silencing reduced cell growth, even though its overexpression had not impact on cancer cell proliferation.^[25] However, analysis of 3D models does take longer and thus we used lentiviral transduction with shRNA oligos to produce stable TNS4 knockdowns. This allowed spheroid growth to be monitored for 7 days.

We first tested for changes in adhesiveness to both acellular stroma composed of collagen type I and CAFs following TNS4 knockdown. We observed that shTNS4 transfected cells show significantly reduced adhesion to CAFs and slightly decreased adhesion to collagen type I. This effect could be due to a disturbance in molecular mechanosensors where TNS4 is located.^[26] The receptor for collagen type I, an integrin $\alpha 1 \beta 1$ heterodimer, has its expression controlled by C-Myc and this is one of the events regulating cancer progression.^[27,28] It is possible that at different

stages of their neoplastic progression, as HT29 and SW480 undergo TNS4 knockdown, expression of integrin $\alpha 1 \beta 1$ heterodimers is deregulated, resulting in significantly reduced adhesiveness to collagen type I. Adhesion of CRC cells to CAFs might also be mediated by the multi-molecular adhesome of integrin B1 heterodimers. The cytoplasmic tails of integrins are bound to the C-terminus phosphotyrosine-binding domain of TNS4 which in turn forms a complex with several other proteins including actin.^[29–32] Therefore, it is possible that removing TNS4 protein by gene knockdown could disturb the stability of the integrin B1 adhesome and its ability to bind to CAF-secreted fibronectin.

We next tested whether TNS4 expression could affect cell proliferation in spheroid models. Interestingly it appears to vary according to the spheroid morphology produced. In SW620, SW480, and LS1034, which naturally produce irregular shaped and loose spheroids when grown in 3D, a reduction in TNS4 expression resulted in decreased cell proliferation. In contrast, HCT116 and HT29, which naturally produce tight spheroids, shTNS4 transduction caused a significant increase in proliferation. The data were consistent for both fluorescence measurements and spheroid volumetric analysis indicating that the observations were not technical artefacts. This change in cell

Table 2. Statistical analysis of volume measurements at day 7 for spheroids composed of CRC cell lines with and without CAFs. For each condition $N = 12$ replicates and results are representative of two experiments. Two-way ANOVA statistical test with multiple comparisons by Tukey's test was performed, a p -value < 0.05 was considered statistically significant.

Volumetry multiple comparisons at day 7		
	Mean diff.	Adjusted p value
A)		
DLD1 shTNS4 vs. DLD1 shTNS4 + CAFs	-0.1372	0.9321
DLD1 shTNS4 vs. DLD1 shLUC	1.86	<0.0001
DLD1 shTNS4 + CAFs vs. DLD1 shLUC + CAFs	-0.7782	<0.0001
DLD1 shLUC vs. DLD1 shLUC + CAFs	-2.775	<0.0001
B)		
HCT116 shTNS4 vs. HCT116 shTNS4+CAFs	-1.801	<0.0001
HCT116 shTNS4 vs. HCT116 shLUC	-0.7325	<0.0001
HCT116 shTNS4 + CAFs vs. HCT116 shLUC + CAFs	-1.911	<0.0001
HCT116 shLUC vs. HCT116 shLUC + CAFs	-2.979	<0.0001
C)		
HT29 shTNS4 vs. HT29 shTNS4+CAFs	0.832	<0.0001
HT29 shTNS4 vs. HT29 shLUC	-0.5574	<0.0001
HT29 shTNS4 + CAFs vs. HT29 shLUC + CAFs	-0.2921	<0.0001
HT29 shLUC vs. HT29 shLUC + CAFs	1.097	<0.0001

proliferation observed in compact spheroids could be related to the effects on spheroid compactness and cell adhesiveness by disturbing molecular mechanosensors at the focal adhesion complex where TNS4 is situated and altering focal adhesion kinase (FAK)-related contact inhibition. An association between phosphorylated FAK and nuclear TNS4 expression has been previously reported in metastases of CRC cases,^[33] and it was suggested that the two pathways may interact. It is possible that the fine balance existing between the extracellular matrix and cell-to-cell interactions, FAK activation could be influenced by a downregulation of TNS4 to alter cell proliferation.^[34]

When CAFs were added to the spheroid cultures, as documented in other studies, this supported growth of CRC cells thereby validating our 3D spheroid co-culture model.^[17] Interestingly, in this context, a growth advantage is also seen for shTNS4 + CAFs in cell lines forming compact spheroids (DLD1, HCT116, and HT29), but not in loose spheroids formed by SW620, SW480, and LS1034. This data could suggest a novel role for TNS4 in intercellular interactions. Integrins have been reported to form heterotypic complexes with adhesion molecules in adjacent cells and this may form part of a contact inhibition mechanism.^[29] Alternatively, the explanation may lie in differences in the diffusion rates of CAF-secreted growth factors, such as TGF β ,^[35] in tight versus loose spheroids.

When investigating invasion and matrix degradation of 3D spheroids, we observed that, in two cell lines, knockdown of TNS4 replicated the data seen in 2D analysis. Validating the

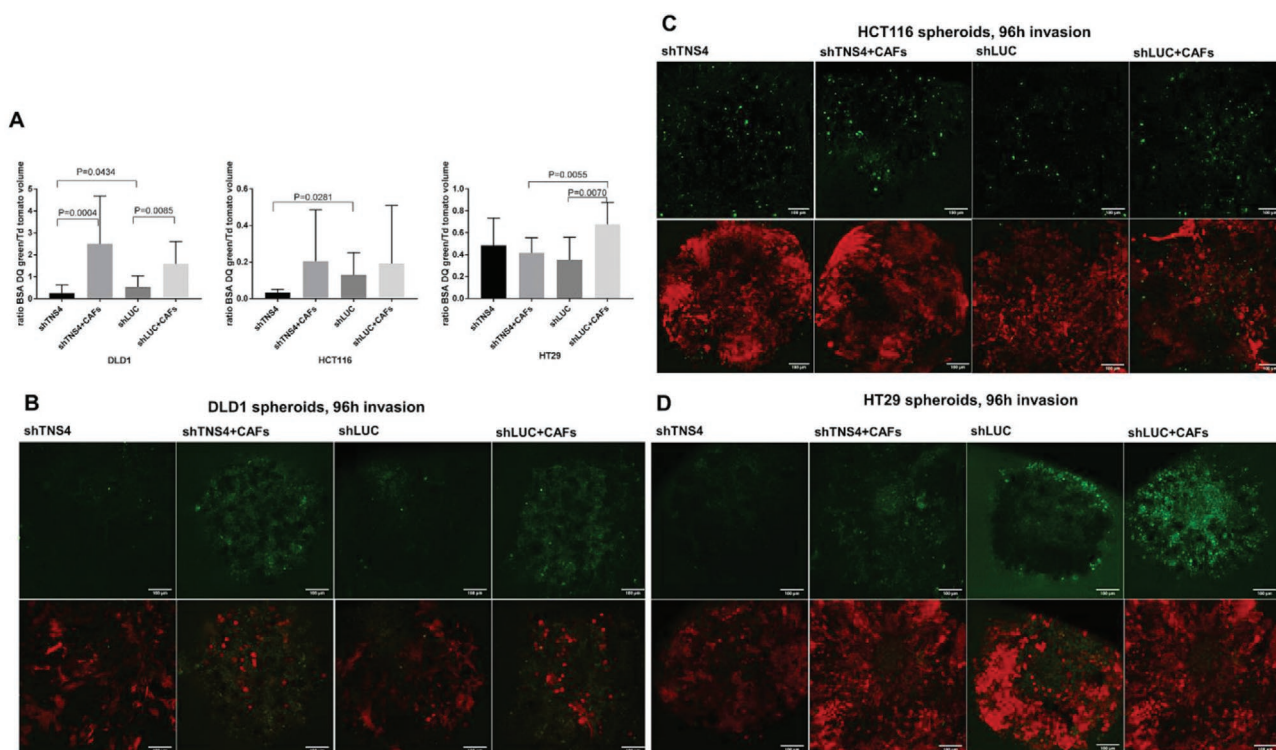


Figure 5. A) 96h measurement of extracellular matrix degradation in 3D spheroid invasion assay using DQ BSA green. Mann–Whitney t -test was used for comparisons between two groups of non-parametric data. Exact p -values shown are representative of two independent experiments. Where non-indicated, differences were non-significant. Representative images of Z-stack slice of 3D spheroids for B) DLD1, C) HCT116, and D) HT29. In B, C, D, upper row depicts DQ BSA green fluorescence and lower row a projection of the maximum intensity of all slices in the confocal microscopy Z-stack.

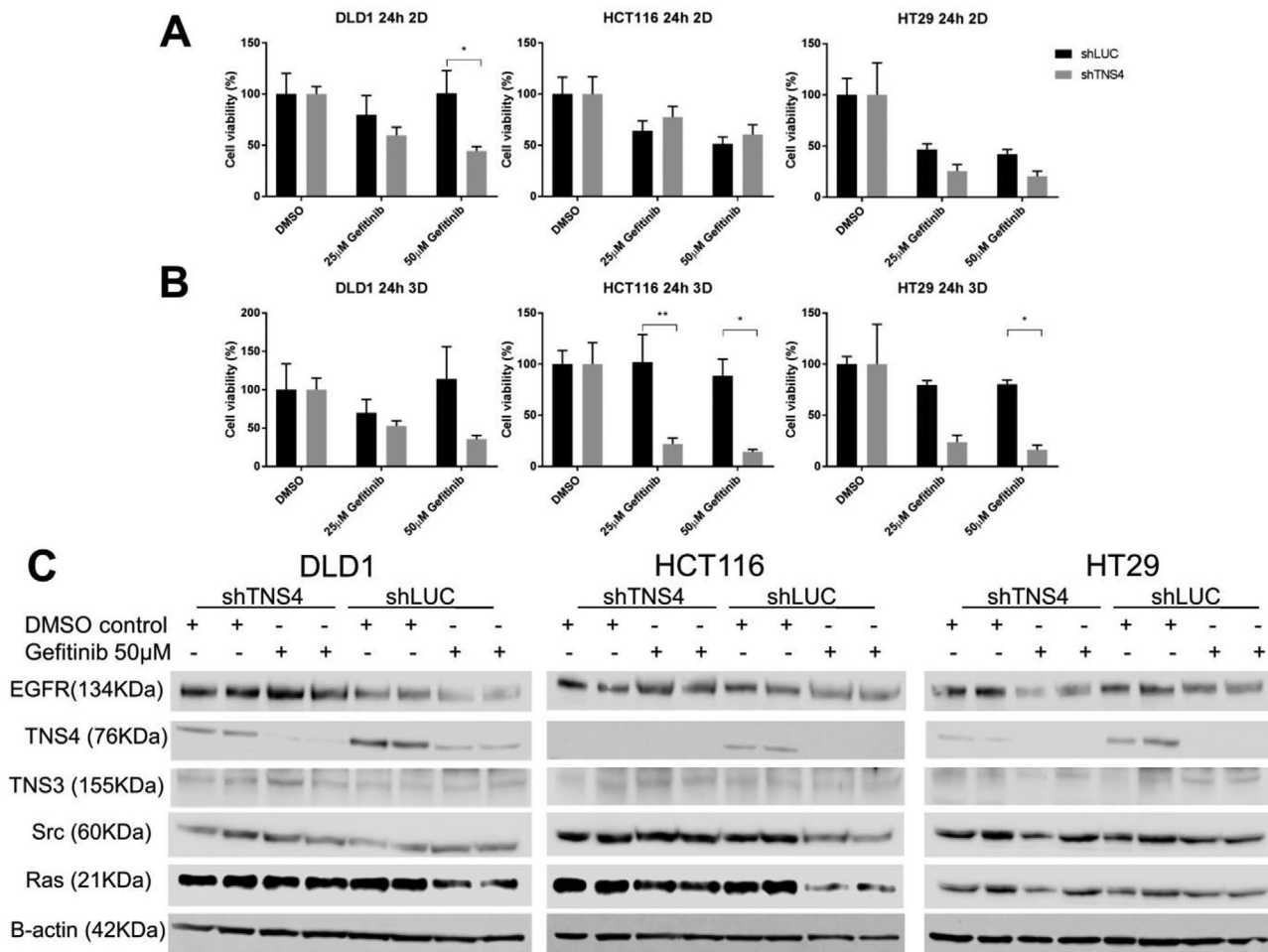


Figure 6. Chemosensitivity of shTNS4 and shLUC CRC cell lines in A) 2D and B) 3D conditions. Western blot protein detection of EGFR, TNS4, TNS3, Src, and Ras in shTNS4 and shLUC CRC cells, treated with Gefitinib 50 μ M for 24 h and respective controls, in two samples obtained from independent experiments. *p*-values indicating statistically significant differences are marked by * (*p* < 0.05) or ** (*p* < 0.01).

effects of TNS4 in these more sophisticated models supports the role of TNS4 in carcinogenesis. When CAFs were added to the 3D spheroids, as expected, increased invasiveness was observed. This effect has been explained by CAFs-directed assembly of fibronectin and induction of integrins α V and β 3.^[36] Furthermore, CAFs have also been described to increase contractility and traction forces in the ECM, mediated by non-muscle myosin II and platelet-derived growth factor α , which are then transmitted through α 5 β 1 integrin to produce an alignment of the fibronectin matrix. Aligned fibronectin matrix features in invasion sites in prostatic and pancreatic carcinomas.^[37] The effect of TNS4 knockdown in the co-culture model was broadly in-line with the effect seen in the 3D monoculture in as much as there was a reduction in matrix degradation but it was not quite as marked. Interestingly, in HT29, whilst the monoculture had shown no effect following TNS4 knockdown, in the 3D co-culture, invasion was significantly reduced in shTNS4 + CAFs spheroids when compared to shLUC + CAFs. These observations were made on several repeated experiments although we do not currently have an explanation, but suspect it could be due to the wild-type status of KRAS gene in HT29 and its different EGFR signaling potency.

Given our previous data demonstrating the involvement of TNS4 in EGFR/KRAS/MAPK signaling,^[5,38,39] we have used our model to test this in 3D spheroids. We also tested whether TNS4 could modulate the activity of anti-EGFR therapies by using gefitinib, which is an inhibitor of the EGFR kinase domain. Our results show a reduction of TNS4 levels with gefitinib treatment, thereby confirming TNS4 is part of this pathway and suggesting the blockade of EGFR tyrosine kinase domain could lead to TNS4 increased degradation.

It has been shown that TNS4 stabilizes EGFR by reducing its ligand-induced degradation via a reduction in its ubiquitination, but not EGF-induced tyrosine phosphorylation of EGFR.^[40] In shTNS4 spheroids, EGFR would be more unstable and easily degraded upon ligand-binding. Lower levels of active EGFR would also lead to increased sensitivity to its inhibitor gefitinib, which we have observed in DLD1 and HT29. By performing gefitinib chemosensitivity test using shTNS4 and shLUC cells, we have observed a reduction in cell viability with TNS4 knockdown in both 2D and 3D conditions. This supports the notion that TNS4 is an important downstream component of the EGFR signaling pathway and raises the possibility of an anti-TNS4 therapy being used in combination with anti-EGFR

therapies. A recent study has also demonstrated that TNS4 is significantly downregulated by cetuximab (anti-EGFR immunotherapy) and put forward the possibility that TNS4 suppression could be used in cetuximab-refractory CRC patients with *KRAS* activating mutations.^[41]

We recognize that the 3D spheroid tumor microenvironment we have created with heterotypic interactions between CRC cells and CAFs is far from being ideal and the presence of immune cells and permeable vasculature would be an important addition to our model. Other types of models, such as patient-derived recellularized CRC scaffolds^[21,42] or well-defined hydrogel-based spheroids^[43] may be useful alternatives to recreate the CRC tumor microenvironment in vitro, as well as those with the addition of lymphoid^[44] or endothelial^[45] cells to increase the model complexity.

In summary, we have hereby used a novel methodology to mimic an enriched 3D colorectal tumor microenvironment and demonstrate a role for TNS4 in the dynamics of cell adhesion, 3D spheroid proliferation, invasion and EGFR inhibitor resistance. These results suggest TNS4 has a valuable role as an effector in early stage metastasis, likely associated with its mechanosensing properties and involvement in heterotypic interactions at the focal adhesion complex. Furthermore, TNS4 inhibition might improve the efficacy of anti-EGFR therapy, by increasing its chemosensitivity.

4. Experimental Section

Cell Culture: CAFs were isolated from human colon carcinoma resection specimens following 2.4 U mL⁻¹ dispase and 100 U mL⁻¹ collagenase type II (both from Invitrogen) disaggregation of tumor fragments and digestion for 2 h at 37 °C. Cells were cultured in Dulbecco's Modified Eagle Medium (DMEM, Gibco) supplemented with 20% heat-inactivated fetal bovine serum (FBS, Gibco), 2 mM L-glutamine, 0.1% hydrocortisone (w/v), 0.75% bovine insulin (w/v).

All cell lines used in this study were obtained from the American Tissue Culture Collection (ATCC) and used for experiments up to passage 30. SW620^{ΔCten} is derived from SW620 submitted to TNS4 deletion by CRISPR-Cas9.^[46]

HEK293T, DLD1, HCT116, SW480, SW620, SW620^{ΔCten} were maintained in 2D cell culture in DMEM (Gibco) supplemented with 10% heat-inactivated FBS (Gibco), 2 mM L-glutamine and incubated at 37 °C, 5% CO₂. Cells were regularly passaged by dissociation with Trypsin-Ethylenediaminetetraacetic acid (Trypsin-EDTA) 0.25% (Sigma Aldrich) every 2–3 days.

HT29 was maintained in McCoy's 5A medium supplemented with 10% FBS and 2 mM L-glutamine. LS1034 was maintained in Roswell Park Memorial Institute (RPMI) 1640 supplemented with 10% FBS and 2 mM L-glutamine. Gefitinib (Sigma Aldrich, Y001813) was diluted to the concentration of 100 μM in dimethyl sulfoxide (DMSO) and subsequently dissolved in cell culture media to concentrations of 50 and 25 μM. Cell viability was measured in six replicates, by using a Fluorostar Omega plate fluorescence plate reader (540 nm excitation, 590 nm emission) after incubation with 10% Presto Blue (Life Technologies) for 1 h at 37 °C, 5% CO₂.

Lentivirus Production and Transduction: The lentiviral plasmid components were acquired from Addgene: Transfer plasmids: Rix-PGK-Tom-W (#25 813), FUGW (#14 883), and PLKO.1 TRC (# 10 878); Packaging plasmid: psPAX2 (#12 260) and Envelope: pMD2.G (#12 259).

The short hairpin RNA (shRNA) for TNS4 and LUC (Luciferase) knockdown were selected from the RNAi consortium shRNA library (<https://www.broadinstitute.org/rnai-consortium/rnai-consortium-shrna-library>).

The shRNA oligos (Table S1, Supporting Information) were annealed at 95 °C for 4 min in a PCR thermal cycler and slowly cooled down overnight. The annealed oligos were phosphorylated, ligated into pLKO.1-TRC, transformed in chemocompetent E.coli (New England Biolabs), isolated by miniprep, and double-digested with restriction enzymes AgeI and EcoRI (both New England Biolabs). Correctly inserted oligos were confirmed by restriction enzyme double-digestion of the resulting vectors with EcoRI and NcoI and Sanger sequencing.

Viral particles were packaged in HEK293T cells seeded at a density of 1.5 × 10⁶ per 10 cm petri dishes in a proportion of 24 μL Fugene 6 (Promega, E2691) in 136 μL serum-reduced OPTI-MEM (Gibco, Invitrogen) to 2 μg pLKO.1 shRNA plasmid: 1500 ng psPAX2 packaging plasmid (Addgene #12 260): 500 ng pMD2.G envelope plasmid (Addgene #12 259) to 40 μL serum-reduced OPTI-MEM. 72 h after transfection, shRNA lentiviruses were concentrated by ultracentrifugation at 10000 × g, 4 °C, 4 h in a 10% sucrose buffer.^[47] Lentivirus titers were examined by Lenti-go stix quick test (Takara Bio, 631 280) according to the manufacturers' instructions, using the freely mobile app (Lenti-X GoStix) to determine titer concentrations.

CRC cell lines were first transduced with PLKO.1 shTNS4/shLUC lentivirus and selected with Puromycin (Sigma Aldrich, p8833) at a dose that killed 100% of non-transduced control cells over a 7-day period, followed by transduction with TdTomato lentivirus at excessive multiplicity of infection (MOI) to ensure complete transduction efficiency. Cancer-associated fibroblasts were transduced with FUGW lentivirus to induce EGFP expression also at excessive MOI. Maintenance of complete transduction efficiency was routinely inspected by observation of TdTomato and EGFP expression across several passages, using a wide-field Nikon TiE fluorescence microscope.

Protein Extraction and Western Blot: Cells were washed with ice-cold PBS and incubated on ice for 10 min with radioimmunoprecipitation assay (RIPA) buffer (Invitrogen) with protease and phosphatase inhibitor (Pierce, ThermoFisher) diluted to 1x. Resulting cell lysates were centrifuged at 16 000g, at 4 °C for 30 min and the supernatant transferred to a new eppendorf tube. A bicinchoninic acid assay (BCA) assay was performed to determine protein quantification of the supernatant.

For Western blotting, 40 μg of protein mixed with 25%(v/v) NuPAGE LDS Sample buffer(4x) and 10%(v/v) reducing sample buffer (10x) were denatured at 95 °C for 5 min, incubated in ice for 5 min and then loaded into a pre-cast gel (NuPAGE 4–12% Bis-Tris Protein Gels, Invitrogen). Gel electrophoresis was performed for 90 min at 125 V. The resulting gel was immunoblotted onto a nitrocellulose membrane (Amersham, GE Healthcare Life Sciences) at 25 V for 30 min, using the Trans-Blot Transfer system (BIO-RAD).

After confirming transfer by Ponceau Red staining, the membrane was blocked with 5% skimmed milk (Sigma-Aldrich) in tris-buffered saline (TBS) for 1 hour with gentle agitation at room temperature. The membrane was then incubated overnight with primary antibodies at 4 °C with gentle agitation (dilutions and suppliers listed on supplementary table 2) and then washed 3 × 5 min with tris-buffered saline, 0.1% tween 20 (TBST). The hybridized membrane was incubated with the respective IRDYE-conjugated secondary antibody (Donkey anti-mouse or anti-rabbit 800CW) for 1 h at room temperature, using the blocking solution as the diluent. The membrane was further washed 3 × 5 min in TBST and infra-red fluorescence detected with the Li-Cor Odyssey Blot scanner. Densitometry of the western blot bands was performed with Image studio lite software (LI-COR). Original imaged blots are shown in the negative image of the captured fluorescence light for better contrast without incurring in any modifications that could bias the perceived band intensity.

3D Spheroid Formation, Volumetry, and Fluorescence Readings: Cell suspensions of the TdTomato expressing colorectal cell lines, their shTNS4 and shLUC expressing variants, were seeded in 12-replicates in Ultra-low attachment 96-well plates (CLS4515, Corning) at 2.0 × 10⁴ cells mL⁻¹ in a final volume of 100 μL alone or in a 1:1 mix with CAFs, in Fluorobrite DMEM supplemented with 10% FBS and 4 mM L-glutamine. The plates were centrifuged at 200 g for 5 min, at acceleration 7 and deceleration 7 in a Megafuge 16 centrifuge (ThermoScientific).

Spheroid or aggregate formation was confirmed in 24–48 h and daily measurements of fluorescence were taken in a Fluostar Omega plate reader (BMG Labtech) set to perform bottom readings, at 544 nm excitation and 590 nm emission wavelength, gain 2500. Fluorescence readings were normalized to day 1 to account for initial differences in seeded cell numbers. Brightfield images of spheroids were taken daily for volumetry quantification using a widefield inverted microscope (Nikon TiE). Volumetry analysis was performed using Image J Wand tracing tool in eight-connected mode to determine the area of each spheroid. Mean spheroid radius was determined by assuming an approximation to the area of the circle and from there inferred the volume of the spheroid, as an approximation to the volume of a sphere.

Adhesion Assays: Adhesion assays to collagen type I and CAFs were performed to assess adhesiveness of shTNS4 cells versus its shLUC control. 96-well flat bottom plates (Costar) were coated with 100 μ L of 0.3 mg mL⁻¹ of rat tail collagen type I (Corning) diluted in PBS, 0.02M NaHO. Plates were incubated overnight at 37 °C. For adhesion to CAFs, 96 well plates were seeded with 1000 CAFs per well and incubated overnight at 37 °C. CRC cell lines were added to coated or CAF seeded plates at a density of 2.0×10^4 cells per well, and incubated for 2 h. Half of the wells containing shTNS4 and shLUC cells were washed 3x with PBS and then incubated with complete fluorobrite DMEM for 15 min. Fluorescence values at 544–590 nm excitation-emission were read in a Fluostar Omega plate reader. After subtracting background fluorescence, a ratio of washed to non-washed was used to determine cell adhesion.

3D Spheroid Invasion Assay: At day 3 of spheroid formation, spheroids were transferred to a chilled flat-bottomed 96-well plate coated with 50 μ L per well of Cultrex BME RGF (Trevigen) at 6 mg mL⁻¹ and overlaid with another 50 μ L per well of Cultrex and 100 μ L of complete Fluorobrite DMEM supplemented with 80 ng mL⁻¹ human recombinant EGF as a chemoattractant. For extracellular matrix degradation analysis, DQ BSA-Green was added to Cultrex at 30 μ g mL⁻¹ as previously described.^[48]

Spheroids were imaged at 96 h of invasion by confocal microscopy, performing Z-stacks with 3 μ m thick slices using 488 and 568 nm lasers. The volume of each fluorescent component was calculated on Image J given by multiplying the thresholded area (obtained by the Otsu method on the Image J threshold menu options) of each slice by its thickness, using a macro plugin freely available from <http://www.optinav.info/MeasureStack.htm>. A ratio of the measured DQ BSA green per TdTomato fluorescent volume was used as an estimation of ECM degradation normalized to the volume of cancer cells.

Statistical Analysis: Analysis of proliferation and volumetry assays was performed on GraphPad Prism version 7 by two-way ANOVA with multiple mean comparisons by Tukey test. Comparisons between two groups of non-parametric values were performed by Mann–Whitney test. Statistical significance was considered for values of $p < 0.05$.

Supporting Information

Supporting Information is available from the Wiley Online Library or from the author.

Acknowledgements

The authors acknowledge financial support from the Nottingham Molecular Pathology Node – Medical Research Council, United Kingdom grant RA4852. The authors would like to thank Dr. Kenton Arkill for the valuable technical advice on setting up the 3D image analysis for the spheroid model.

Conflict of Interest

The authors declare no conflict of interest.

Author Contributions

T.P.R. conducted all the experimental work, analyzed data, and drafted the manuscript. S.S. established the CAFs line and optimized the spheroid co-culture system, M.I. reviewed and edited the manuscript. All authors read and approved the final manuscript.

Keywords

cancer invasion, colorectal cancer, Cten, EGFR inhibitor, in vitro models, tensins

Received: January 27, 2020

Revised: April 7, 2020

Published online: May 10, 2020

- [1] S. H. Lo, *Int. J. Biochem. Cell Biol.* **2004**, *36*, 31.
- [2] J. Ivaska, *Nat. Cell Biol.* **2012**, *14*, 981.
- [3] A. Albasri, M. Aleskandarany, A. Benhasouna, D. G. Powe, I. O. Ellis, M. Ilyas, A. R. Green, *Breast Cancer Res. Treat.* **2011**, *126*, 47.
- [4] A. Albasri, R. Seth, D. Jackson, A. Benhasouna, S. Crook, A. S. Nateri, R. Chapman, M. Ilyas, *J. Pathol.* **2009**, *218*, 57.
- [5] S. Al-Ghamdi, A. Albasri, J. Cachat, S. Ibrahim, B. A. Muhammad, D. Jackson, A. S. Nateri, K. B. Kindle, M. Ilyas, *PLoS One* **2011**, *6*, e20919.
- [6] J. Chen, Y. Zhang, G. Deng, J. Ma, X. Wu, Y. Qu, S. Zeng, *Zhong Nan Da Xue Xue Bao. Yi Xue Ban* **2014**, *39*, 1233.
- [7] C. Sjoestroem, S. Khosravi, G. Zhang, M. Martinka, G. Li, *PLoS One* **2013**, *8*, e80492.
- [8] K. Aratani, S. Komatsu, D. Ichikawa, T. Ohashi, M. Miyamae, W. Okajima, T. Imamura, J. Kiuchi, K. Nishibeppu, T. Kosuga, H. Konishi, A. Shiozaki, H. Fujiwara, K. Okamoto, H. Tsuda, E. Otsuji, *Oncotarget* **2017**, *8*, 84112.
- [9] S. Sawazaki, T. Oshima, K. Sakamaki, T. Aoyama, T. Sato, M. Shiozawa, T. Yoshikawa, Y. Rino, T. Imada, M. Masuda, *In Vivo (Brooklyn)*. **2017**, *31*, 1065.
- [10] K. Sakashita, K. Mimori, F. Tanaka, Y. Kamohara, H. Inoue, T. Sawada, K. Hirakawa, M. Mori, *Ann. Surg. Oncol.* **2008**, *15*, 2606.
- [11] H. Sasaki, H. Yukiue, Y. Kobayashi, I. Fukai, Y. Fujii, *Tumor Biol.* **2003**, *24*, 271.
- [12] H. Sasaki, S. Moriyama, K. Mizuno, H. Yukiue, A. Konishi, M. Yano, M. Kaji, I. Fukai, M. Kiriama, Y. Yamakawa, Y. Fujii, *Lung Cancer* **2003**, *40*, 151.
- [13] A. Asiri, T. P. Raposo, A. Alfahed, M. Ilyas, *Int. J. Exp. Pathol.* **2019**.
- [14] A. Asiri, M. S. Toss, T. P. Raposo, M. Akhlaq, H. Thorpe, A. Alfahed, A. Asiri, M. Ilyas, *Pathol. Int.* **2019**, pin. 12811.
- [15] A. Albasri, S. Al-Ghamdi, W. Fadhil, M. Aleskandarany, Y.-C. Liao, D. Jackson, D. N. Lobo, S. H. Lo, R. Kumari, L. Durrant, S. Watson, K. B. Kindle, M. Ilyas, *Oncogene* **2011**, *30*, 2997.
- [16] I. A. Khawar, J. K. Park, E. S. Jung, M. A. Lee, S. Chang, H.-J. Kuh, *Neoplasia* **2018**, *20*, 800.
- [17] S.-A. Kim, E. K. Lee, H.-J. Kuh, *Exp. Cell Res.* **2015**, *335*, 187.
- [18] M. J. Lamberti, M. Rettel, J. Krijgsveld, V. A. Rivarola, N. B. Rumie Vittar, *Cell. Oncol.* **2019**.
- [19] S. Nath, G. R. Devi, *Pharmacol. Ther.* **2016**, *163*, 94.
- [20] O. I. Hoffmann, C. Ilmberger, S. Magosch, M. Joka, K.-W. Jauch, B. Mayer, *J. Biotechnol.* **2015**, *205*, 14.
- [21] F. Sensi, E. D'Angelo, M. Piccoli, P. Pavan, F. Mastrotto, P. Caliceti, A. Biccari, D. Corallo, L. Urbani, M. Fassan, G. Spolverato, P. Riello, S. Pucciarelli, M. Agostini, *Cancers*. **2020**, *12*, 681.
- [22] A. Labernadie, T. Kato, A. Brugués, X. Serra-Picamal, S. Derzsi, E. Arwert, A. Weston, V. González-Tarragó, A. Elosgui-Artola,

- L. Albertazzi, J. Alcaraz, P. Roca-Cusachs, E. Sahai, X. Trepas, *Nat. Cell Biol.* **2017**, 19, 224.
- [23] S. Cattin, L. Ramont, C. Rüegg, *Frontiers in Bioengineering and Biotechnology* **2018**, 6.
- [24] Y. C. Liao, N. T. Chen, Y. P. Shih, Y. Dong, H. Lo Su, *Cancer Res.* **2009**.
- [25] S.-Y. Hong, Y.-P. Shih, A. Lo, S. H. Lo, *Biochimica et Biophysica Acta (BBA) - Molecular Cell Research* **2019**, 1866, 450.
- [26] D. T. Haynie, *Proteins: Struct., Funct., Bioinf.* **2014**, 82, 1113.
- [27] S. Boudjadi, G. Bernatchez, B. Séricourt, M. Beauséjour, P. H. Vachon, J. C. Carrier, J. F. Beaulieu, *Cancers* **2017**, 9, 96.
- [28] S. Boudjadi, J. C. Carrier, J. F. Groulx, J. F. Beaulieu, *Oncogene* **2016**, 35, 1671.
- [29] A. Manninen, M. Varjosalo, *Proteomics* **2017**, 17, 1600022.
- [30] G. Muharram, P. Sahgal, T. Korpela, N. DeFranceschi, R. Kaukonen, K. Clark, D. Tulasne, O. Carpén, J. Ivaska, *Dev. Cell* **2014**.
- [31] M. Katz, I. Amit, A. Citri, T. Shay, S. Carvalho, S. Lavi, F. Milanezi, L. Lyass, N. Amariglio, J. Jacob-Hirsch, N. Ben-Chetrit, G. Tarcic, M. Lindzen, R. Avraham, Y. C. Liao, P. Trusk, A. Lyass, G. Rechavi, N. L. Spector, S. H. Lo, F. Schmitt, S. S. Bacus, Y. Yarden, *Nat. Cell Biol.* **2007**.
- [32] D. A. Calderwood, Y. Fujioka, J. M. de Pereda, B. Garcia-Alvarez, T. Nakamoto, B. Margolis, C. J. McClade, R. C. Liddington, M. H. Ginsberg, *Proc. Natl. Acad. Sci. USA* **2003**, 100, 2272.
- [33] A. Albasri, W. Fadhil, J. H. Scholefield, L. G. Durrant, M. Ilyas, *Anti-cancer Res.* **2014**, 34, 3969.
- [34] C. Gerard, A. Goldbeter, *Interface Focus* **2014**, 4, 20130075.
- [35] L. J. A. C. Hawinkels, M. Paauwe, H. W. Verspaget, E. Wiercinska, J. M. van der Zon, K. van der Ploeg, P. J. Koelink, J. H. N. Lindeman, W. Mesker, P. ten Dijke, C. F. M. Sier, *Oncogene* **2014**, 33, 97.
- [36] Y. Attieh, A. G. Clark, C. Grass, S. Richon, M. Pocard, P. Mariani, N. Elkhatib, T. Betz, B. Gurchenkov, D. M. Vignjevic, *J. Cell Biol.* **2017**, 216, 3509.
- [37] B. Erdogan, M. Ao, L. M. White, A. L. Means, B. M. Brewer, L. Yang, M. K. Washington, C. Shi, O. E. Franco, A. M. Weaver, S. W. Hayward, D. Li, D. J. Webb, *J. Cell Biol.* **2017**, 216, 3799.
- [38] H. Thorpe, M. Akhlaq, D. Jackson, S. Al Ghamdi, S. Storr, S. Martin, M. Ilyas, *Int. J. Exp. Pathol.* **2015**, 96, 362.
- [39] S. Al-Ghamdi, J. Cachat, A. Albasri, M. Ahmed, D. Jackson, A. Zaitoun, N. Guppy, W. R. Otto, M. R. Alison, K. B. Kindle, M. Ilyas, *Pancreas* **2013**, 42, 135.
- [40] S.-Y. Hong, Y.-P. Shih, T. Li, K. L. Carraway, S. H. Lo, *Cancer Res.* **2013**, 73, 5266.
- [41] K. Kim, K. Kang, C. Won, *Cells* **2019**, 8, 878.
- [42] E. D'Angelo, D. Natarajan, F. Sensi, O. Ajayi, M. Fassan, E. Mammano, P. Pilati, P. Pavan, S. Bresolin, M. Preziosi, R. Miquel, Y. Zen, S. Chokshi, K. Menon, N. Heaton, G. Spolverato, M. Piccoli, R. Williams, L. Urbani, M. Agostini, *Cancers.* **2020**, 12, 364.
- [43] G. Rijal, W. Li, *Sci. Adv.* **2017**, 3, e1700764.
- [44] T. E. Schnalzger, M. H. Groot, C. Zhang, M. H. Mosa, B. E. Michels, J. Röder, T. Darvishi, W. S. Wels, H. F. Farin, *EMBO J.* **2019**, 38.
- [45] M. Zoetemelk, M. Rausch, D. J. Colin, O. Dormond, P. Nowak-Sliwinska, *Sci. Rep.* **2019**, 9, 7103.
- [46] H. Thorpe, A. Asiri, M. Akhlaq, M. Ilyas, *Mol. Carcinog.* **2017**, 56, 2601.
- [47] W. Jiang, R. Hua, M. Wei, C. Li, Z. Qiu, X. Yang, C. Zhang, *Sci. Rep.* **2015**, 5, 13875.
- [48] C. Goertzen, D. Eymael, M. Magalhaes, *Biol. Proced. Online* **2018**, 20, 20.